

Article

Test Method for Thermal Characterization of Li-Ion Cells and Verification of Cooling Concepts

Rouven Christen *, Gerhard Rizzo, Alfred Gadola and Max Stöck

Institute for Development of Mechatronic Systems, NTB Interstate University of Applied Sciences of Technology, Werdenbergstrasse 4, CH-9471 Buchs, Switzerland; gerhard.rizzo@ntb.ch (G.R.); alfred.gadola@ntb.ch (A.G.); max.stoeck@ntb.ch (M.S.)

* Correspondence: rouven.christen@ntb.ch; Tel.: +41-81-755-34-35; Fax: +41-81-756-54-34

Academic Editor: Carlos Ziebert

Received: 29 November 2016; Accepted: 19 January 2017; Published: 26 January 2017

Abstract: Temperature gradients, thermal cycling and temperatures outside the optimal operation range can have a significant influence on the reliability and lifetime of Li-ion battery cells. Therefore, it is essential for the developer of large-scale battery systems to know the thermal characteristics, such as heat source location, heat capacity and thermal conductivity, of a single cell in order to design appropriate cooling measures. This paper describes an advanced test facility, which allows not only an estimation of the thermal properties of a battery cell, but also the verification of proposed cooling strategies in operation. To do this, an active measuring unit consisting of a temperature and heat flux density sensor and a Peltier element was developed. These temperature/heat flux sensing (THFS) units are uniformly arranged around a battery cell with a spatial resolution of 25 mm. Consequently, the temperature or heat flux density can be controlled individually, thus forming regions with constant temperature (cooling) or zero heat flux (insulation). This test setup covers the whole development loop from thermal characterization to the design and verification of the proposed cooling strategy.

Keywords: testing; cell characterization; thermal management; heat generation

1. Introduction

Li-Ion batteries are widely used for different applications due to their high specific energy and power density, excellent coulombic efficiency and low memory effect [1]. Reliability and life-time of a battery system are essential factors to achieve technical and economic success with a product, such as an electric vehicle (EV) or a stationary energy storage system. Despite the very good electrical performance mentioned above, the operating conditions are subject to certain restrictions. For instance, Waldmann et al. [2] reported that Lithium plating is observed if a cell is operated below 25 °C, but also elevated temperatures above 25 °C accelerate other degradation reactions such as solid-electrolyte interphase (SEI) growth, which leads to capacity fade, increase in internal resistance, and, in the worst case, to thermal runaway. An increase in internal resistance caused by elevated temperature was also reported by Bloom et al. [3] and Vetter et al. [4]. Troxler et al. [5] showed that, in the case of a temperature gradient across a single cell, the behavior is dictated by the higher temperature region, and the overall performance is comparable to a cell with higher uniform temperature. In order to avoid these types of degradation, the battery cell has to be kept within a narrow temperature range throughout its operational lifetime. The described effects are even more crucial if a large number of cells are connected in parallel to form a high capacity battery system as used in EV. Any resistance differences caused by temperature variation among the cells within a system can lead to additional undesired effects. As found by Gogoana et al. [6], a 20% variation in the internal resistance of two cells connected in parallel can lead to a 40% reduction in their lifetime.

However, protection of the battery system against changing ambient temperature conditions is not sufficient. Rather, the heat generated within the cell due to resistive losses and change in entropy have to be considered [7,8]. Under certain circumstances, even endothermic behavior can be observed [9]. In order to avoid the above-mentioned temperature induced degradation phenomenon and to prolong the operational lifetime of a battery system, an adequate thermal management system is needed. This was the motivation for the authors to conceive a new method for thermal cell characterization, which delivers all the necessary information on the cell behavior to develop optimized thermal management systems.

In this study, the term thermal behavior includes system parameters such as heat conductivity λ or heat capacity c_p of the cell itself, but also the amount of heat which is generated inside the cell during a given load profile. Additionally, the location at the cell surface where the heat is released to the environment is of great interest. It will be shown that the proper selection of the location where the cooling system is in contact with the battery cell has a great impact on its efficiency. In order to determine this type of thermal cell behavior, localized acquisition of the required quantities is mandatory. Thermal imaging is a possible approach to capture high resolution temperature fields. This type of thermal imaging is usually accomplished through charge/discharge cycles while the cell is under natural convection at a given temperature [10,11]. A major drawback of the thermal imaging method is the lack of information regarding the amount of heat exchanged with its surroundings. Moreover, the method ignores the fact that a cell is usually closely packed inside a battery module. In such a setting, several cells are in contact with each other and the framework of the battery, which has a significant impact on heat flow within the system. On the other hand, the cell global parameters such as heat capacity c_p can be identified precisely using an accelerated rate calorimeter (ARC). However, no information about local differences in heat dissipation is obtained.

A procedure with local heat flux measurements has been proposed by Murashko et al. [12], which was used to determine the thermal conductivity and specific heat capacity of a pouch cell. Similarly, the approach presented in this paper includes the simultaneous acquisition of local temperature and heat flux density. Moreover, using the introduced test rig with the specially developed sensing units enables both quantities to be controlled actively, which allows the reproduction of various packaging situations.

2. Experimental

2.1. System Overview

The test rig described in this paper has the ability to acquire and control heat flux and temperature distribution on the surface of prismatic and pouch cells with a spatial resolution of 25 mm. However, it has to be considered that the thermal coupling between the sensing unit and a pouch cell is more difficult. This is because the pouch cell packaging is not able to withstand the necessary contact forces. Therefore, the first set of experiments presented in this paper was conducted on a prismatic cell. To do this, the cell under test is surrounded by 87 uniformly distributed temperature/heat flux sensor (THFS) units, which are in contact with the battery cell on one side while connected to a heat sink on the other side. The heat sink consists of an aluminum block with integrated cooling channels through which a coolant with the fixed temperature T_{sink} is circulated. The main functionality of the THFS units is to measure the surface temperature of the device under test, as well as the heat flux density flowing from the sample towards the heat sink or vice versa. In addition, either one of the two measured quantities can be used as a feedback signal for a closed loop control as shown in Figure 1. Thus, the two sensor signals are acquired using the according hardware (PXIe-4353 and PXIe-6375, National Instruments, Austin, TX, USA) in a PXI chassis. In order to operate all THFS units used in the test rig, a multi-channel power electronic was designed and built, which can be individually controlled by pulse width modulated (PWM) outputs of a Digital I/O Module (NI PXIe-6537, National Instruments). The data acquisition and the multi-channel

control algorithm is implemented in LabView (Version 15.0.1, National Instruments) and allows each of the 87 THFS units to be operated with individual set points and operation modes. Therefore, two proportional-integral (PI) controllers with their respective parameters are running in parallel. The discrete representation of the controller is yielded through a first-order hold approximation according to Equations (1)–(4):

$$y(k) = b_0 \cdot e(k) + b_1 \cdot e(k-1) + a_1 \cdot y(k-1), \quad (1)$$

$$b_0 = Kr \cdot \left(\frac{T_S}{2 \cdot T_N} + 1 \right), \quad (2)$$

$$b_1 = Kr \cdot \left(\frac{T_S}{2 \cdot T_N} - 1 \right), \quad (3)$$

$$a_1 = 1, \quad (4)$$

where K_r is the proportional gain, K_r/T_N is the integral gain, T_S is the controller sampling time, $e(k)$ and $e(k-1)$ are the current and previous control error, and $y(k)$ and $y(k-1)$ are the current and previous controller output. When switching from one operation mode to the other, the integral term of the controllers is reset in order to avoid wind-up problems. The ability to individually control each of the 87 THFS units permits the comparison and verification of different cooling strategies as described in Section 3.2 below.

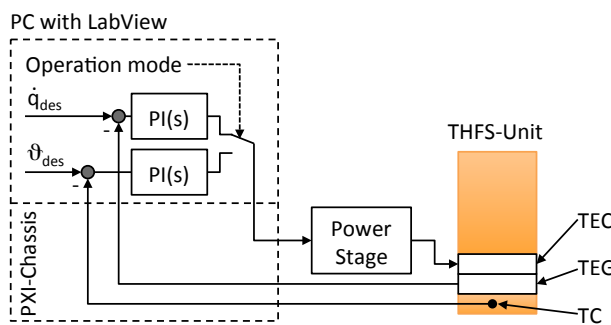


Figure 1. Structure of the implemented control algorithm of one temperature/heat flux sensor (THFS) unit incorporating two different operation modes. PC: personal computer; PI: proportional-integral; TEC: thermo-electric cooler; TEG: thermo-electric generator; and TC: thermocouple.

Operation Mode 1 (constant temperature). *This operation mode is used to keep the battery cell surface temperature at a certain level. To do this, the measured temperature is used as a feedback signal for the closed loop, hence leading to an actively controlled current in the thermo-electric cooler (TEC). At the same time, the heat flux needed to reach the desired cell temperature is measured at each location. If this operation mode is applied to all THFS units at the same time, the heat generation of the battery cell can be quantified and localized. On the other hand, this mode can be applied to a subset of THFS units to simulate a certain cooling strategy, such as constant temperature on the bottom side of the battery cell.*

Operation Mode 2 (constant heat flux). *This operation mode is mainly used to reproduce the situation of realistic packaging scenarios. In contrast to the case above, the measured heat flux density is used here as feedback for the control loop. In this way, a thermal insulation can be realized by applying the desired heat flux density value of $0 \text{ W} \cdot \text{m}^{-2}$. Alternatively, a specific heat transfer coefficient can be simulated by calculating the desired heat flux density according to:*

$$\dot{q}_{des} = \alpha_{sim} \cdot (T_{Bat} - T_v), \quad (5)$$

where T_{Bat} is the measured temperature of the battery cell, T_v is the temperature of the virtual element in contact with the battery and α_{sim} is the heat transfer coefficient to be simulated.

2.2. Temperature/Heat Flux Sensor Unit

In order to locally measure and control temperature and heat flux density, an active sensing unit was developed. This so called temperature/heat flux sensor unit—as shown in the cross-section in Figure 2—is composed of two copper parts, one thermo-couple and two thermo-electric cooler/generator (TEC/TEG). The thermo-couple is installed in the center of the first copper plate, which is only 2 mm thick. The low thickness was chosen to achieve a reasonable response time for the surface temperature measurement. The second element in the stack is the TEG, which is used as the heat flux density sensor. For this purpose, the sensitivity of each TEG element was determined using a specially designed calibration setup. The combined measurement uncertainty of the measured heat flux density is as low as 1.5%. The third element is the TEC, which is used in conjunction with a power stage to actively control the operating mode of the THFS unit. The last element on the far right in Figure 2 is another copper part which is in contact with the heat sink. For the sake of simplicity, the same type of thermo-electric element (TB-31-1.0-2.0 from Kryotherm, Saint-Petersburg, Russia) is used as TEG sensor (Seebeck effect) and TEC actuator (Peltier effect), respectively [13,14].

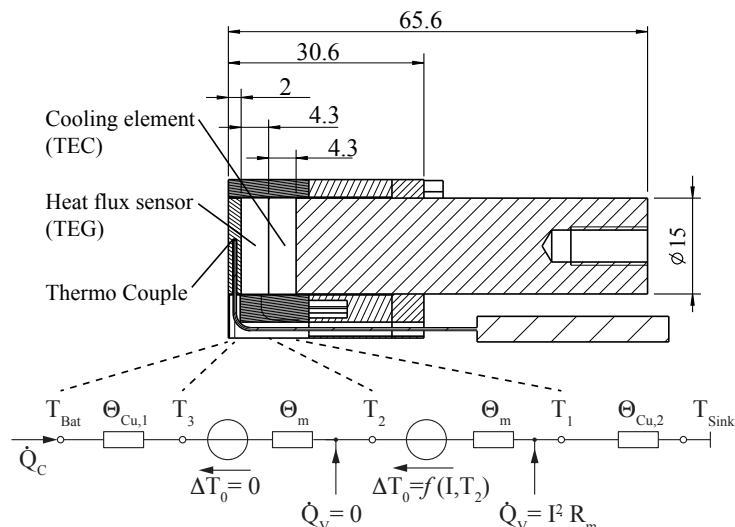


Figure 2. Cross-sectional view of the developed THFS unit with its corresponding equivalent circuit model (ECM) as used for the one-dimensional thermal analysis.

In order to estimate the achievable cooling capabilities for the chosen TEC, a one-dimensional thermal analysis of the THFS was conducted. For that matter, the TEC was modeled as an equivalent circuit model (ECM) according to [15]. The ECM used for the one-dimensional thermal calculations and the relevant parameters are shown in Figure 2 and Table 1, respectively. Thereby, the temperature difference ΔT_0 is a function of the current I and the temperature T_2 given in Kelvin according to:

$$\Delta T_0 = \left(\alpha_m \cdot T_2 \cdot I - \frac{I^2 \cdot R_m}{2} \right) \cdot \Theta_m. \quad (6)$$

Table 1. Equivalent circuit model (ECM) parameters.

Parameter	Description	Value
Θ_m	Thermal resistance of peltier element	$20.3 \text{ K}\cdot\text{W}^{-1}$
R_m	Ohmic resistance of peltier element	1.3Ω
α_m	Seebeck coefficient	$13 \text{ m}\cdot\text{V}\cdot\text{K}^{-1}$
$\Theta_{\text{Cu},1}$	Thermal resistance of left copper part	$0.03 \text{ K}\cdot\text{W}^{-1}$
$\Theta_{\text{Cu},2}$	Thermal resistance of right copper part	$0.30 \text{ K}\cdot\text{W}^{-1}$

The parameters for the TEC model are derived from data sheet values according to Equations (7)–(9) as described in [15]:

$$\Theta_m = \frac{\Delta T_{max}}{I_{max} \cdot U_{max}} \cdot \frac{2 \cdot T_h}{T_h - \Delta T_{max}}, \quad (7)$$

$$R_m = \frac{U_{max} \cdot (T_h - \Delta T_{max})}{I_{max} \cdot T_h}, \quad (8)$$

$$\alpha_m = \frac{U_{max}}{T_h}. \quad (9)$$

It could be shown that the proposed design of the THFS unit is capable of dissipating 1.5 W to 2 W of heat over a wide range of heat sink temperatures, i.e., 0 °C to 30 °C. Taking into account the fact that in some scenarios only some THFS units are used to cool the whole battery cell while the remaining ones are used to simulate thermal insulation, the achieved 2 W seems to be a reasonable order of magnitude. For instance, the total heat loss generated by the investigated prismatic cell under a 2C loading is expected to be about 14 W, which means that only seven THFS units would be needed to dissipate this amount of heat.

3. Results and Discussion

3.1. Thermal Characterization

In this experiment, a 60 Ah high energy density lithium mangan oxid (LMO) cell with physical dimensions of 175 mm × 125 mm × 45 mm is tested. For the characterization measurement, all THFS units are operated in mode 1, which means that the whole surface of the prismatic cell is held constant at 25 °C. Meanwhile, the cell is cycled at a rate of 2C (120 A) between the lower and upper voltage levels of 3.5 V and 4 V, respectively. Comparing these values to the open circuit voltage of the cell, the cycle corresponds to 10% to 80% state of charge (SoC). However, since the 2C rate leads to a considerable voltage drop across the internal resistance, the effective charge during one cycle measured by coulomb counting is 21 Ah, or 36% of the nominal capacity. In order to minimize the effect of variations of the generated heat, the constant voltage phase at the upper boundary of 4 V is kept to a minimum. To do this, the unloading cycle is triggered as soon as the loading current drops below 119 A. The applied load profile is depicted in Figure 3 for reference.

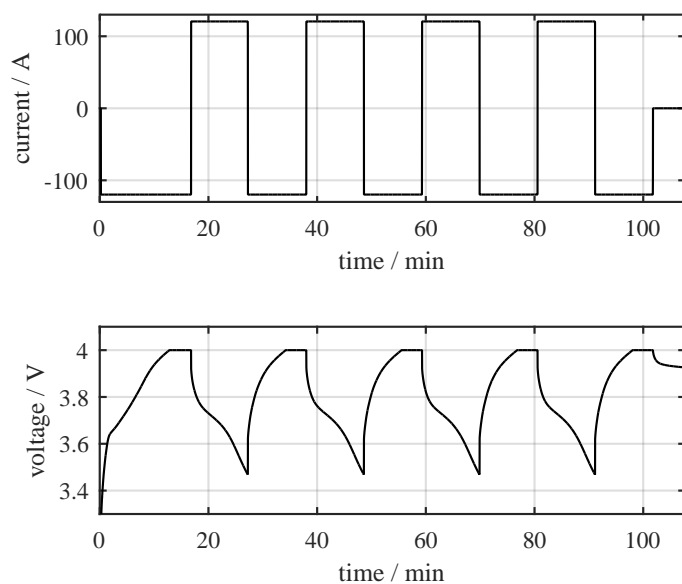


Figure 3. Cell voltage over time for the given 2C loading profile.

At the beginning of the experiment, internal temperature gradients are building up, which leads to the underlying exponential behavior of the heat flux measurements shown in Figure 4. In addition, a superimposed heat flux variation is visible, creating a periodic pattern, which is synchronized with the loading and unloading cycles. It is well known that the heat generation within a Li-ion battery cell is not constant for a given current. According to Liu et al. [16], the generated heat consists of joule heat and reaction heat, which are both dependent, amongst others, on state of charge. However, it can be stated that the system reached a quasi-steady state after about two cycles or after 50 min.

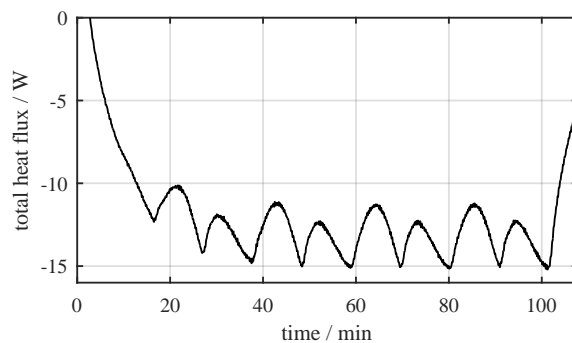


Figure 4. Total measured heat flux over time for the given 2C loading profile.

The post-processing and visualization of the measurement data, as presented below, was conducted in Matlab (Version R2016a, The MathWorks, Inc., Natick, MA, USA). Figure 5 shows the measured heat flux distribution after one hour at steady state with all 87 THFS units operated in temperature controlled mode. Therefore, the total area of the active cooling elements is equal to 19,575 mm², or 27% of the total battery cell surface. Based on these results, the following observations can be formulated:

- The heat flux density on the side faces as well as on the bottom side are close to zero.
- The main part of the heat is almost uniformly released through the large front and rear side.
- The largest heat flux density was measured in close proximity to the positive terminal of the battery cell (see top right corner in Figure 5).

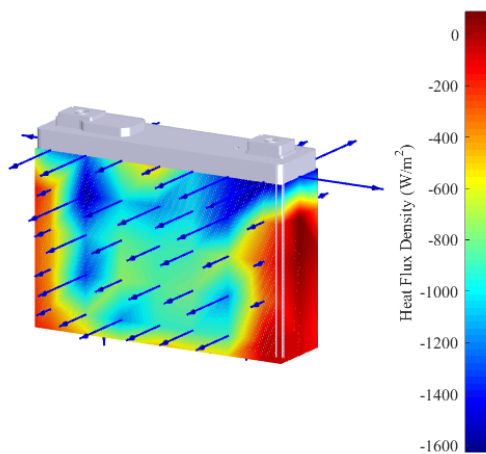


Figure 5. Measured heat flux density for a cell after 60 min cyclic loading with 2C-rate and actively controlled surface temperature of 25 °C.

These results may be partly explained by taking the internal structure of the battery cell into account. In order to do this, the tested prismatic cell is disassembled for further examination. Thereby, the aluminum enclosure is found to contain four stacked pouch cells. The current collectors

for anode and cathode are placed on opposite sides of the pouch cells and are bound together inside the left and right parts of the prismatic cell in Figure 6. Furthermore, they extend to the top side of the enclosure, in order to make a connection to the electrical terminal. Plastic mounting brackets are used for the proper positioning of the pouch cell stack within the enclosure. In addition, the plastic parts act as electrical insulation between the current collectors and the enclosure.

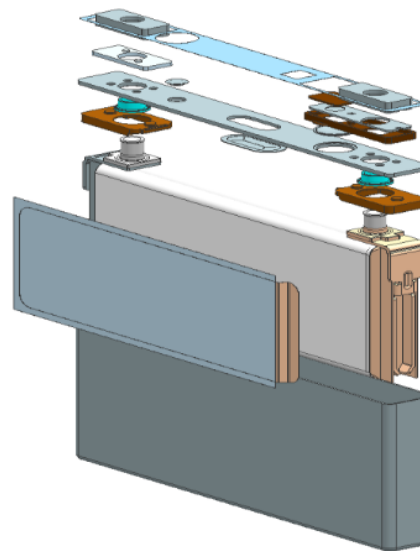


Figure 6. Exploded view drawing of the internal structure of a similar cell as presented in [17].

In general, electrical conductors also exhibit a low thermal resistance. Therefore, a fairly good heat dissipation within the yz -plane (see Figure 7) as well as towards the electrical terminals can be expected. Thus, the low heat flux density on the side faces is a rather surprising result. A possible reason for this observation are the plastic spacers on each side of the pouch cell stack, which introduce an additional thermal resistance to this path (y -direction), resulting in a reduced heat transfer. On the other hand, the high heat flux density measured in close proximity to the electrical terminals can be explained by the low thermal resistance of electrical conductors. Another interesting result is the observed asymmetry between the two electrical terminals. The fact that the positive terminal is in contact with the enclosure is one explanation for the high heat flux density in this region.

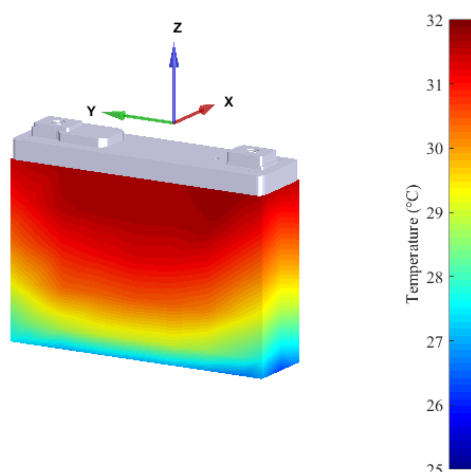


Figure 7. Measured temperature distribution of the prismatic battery cell with a constant temperature of 25 °C on the bottom side and continuous 2C loading.

The above listed observations regarding the heat flux distribution can be qualitatively explained, or even predicted, by examining the internal structure of the cell. However, the extent to which the heat flux density varies between the different sides of the cell is surprisingly large. As shown in Table 2, the average heat flux density on the front and rear sides is higher by a factor of 8, compared to the bottom side. Taking the integral over all THFS units, the average amount of dissipated power is found to be 12.7 W during a discharge and 13.6 W during a charge cycle, respectively. Since the measured values for charge and discharge differ, the generated heat is not only due to joule effect, but indicates the presence of reversible entropy heat. However, the values are slightly lower than the average joule heat dissipated in the internal resistance derived from voltage and current measurements, which is 15.2 W. This difference is due to the fact that some portion of the generated heat is not captured by the THFS units, which will be discussed in more detail in Section 4. Therefore, the presented test rig is not suitable for calorimetric experiments such as ARC, but is able to reveal the heat release capabilities of different areas of the cell.

Table 2. Average heat flux density on the different sides of the battery cell at $t = 60$ min.

Position	Heat Flux Density	Surface Area
Side face (negative)	$219 \text{ W}\cdot\text{m}^{-2}$	5625 mm^2
Side face (positive)	$295 \text{ W}\cdot\text{m}^{-2}$	5625 mm^2
Bottom side	$119 \text{ W}\cdot\text{m}^{-2}$	7875 mm^2
Front side	$964 \text{ W}\cdot\text{m}^{-2}$	$21,875 \text{ mm}^2$
Rear side	$952 \text{ W}\cdot\text{m}^{-2}$	$21,875 \text{ mm}^2$

The described thermal characterization of a battery cell provides useful information for the design of an efficient thermal management system. The results presented in this paper clearly show that the amount of heat which needs to be dissipated is not the only important design criterion. In fact, the proper selection of the location for cooling a battery cell is a crucial point in order to minimize the internal temperature gradients.

3.2. Cooling Strategies

In order to emphasize the point made in the previous section, three tests were performed with different cooling strategies. For such a verification, some THFS units are operated in mode 1 (cooling), while the remaining THFS units are operated in mode 2 (insulation). Therefore, the main path for heat dissipation is the actively cooled face. In the first case, only the bottom side is held at a constant temperature of 25°C , which corresponds to a situation with the cells packed side by side in such a way that the large sides are in contact with each other. From the design point of view, this arrangement is very appealing because it does not require a lot of space and the bottom side of the module is accessible for cooling purposes. Moreover, it is rather simple to accomplish the series connection of the cells by means of short metal straps if the cells have alternating opposing orientations. For these reasons, this configuration is nowadays used in many applications. However, in terms of temperature gradients within the cell, this arrangement is not favorable. The surface temperature distribution after four loading/unloading cycles at a rate of 2C is shown in Figure 7 and Table 3. As can be seen, at a steady state, a temperature gradient of 6.5°C developed over the height of the battery cell.

In order to reach a more homogeneous temperature distribution, the most promising locations for cooling the battery cell seem to be in proximity to the electrical terminals or in the center of the front/rear face. This assumption is made because, in those areas, the dissipated heat flux density is the highest (see Figure 5). In order to confirm this, two more experiments are performed.

During the first experiment, seven THFS units with a total active area of 1575 mm^2 (i.e., 2.7% of the total battery cell surface area, which is $70,750 \text{ mm}^2$) are used to keep the bottom side of the battery cell at a constant temperature of 25°C . For the sake of comparability, a similar active area is chosen for all subsequent sets of experiments. In order to implement the terminal cooling strategy,

a total of eight THFS units is operated in temperature controlled mode: two of them at each terminal on the front and rear side, respectively. Figure 8 shows the temperature field after approximately 120 min of 2C loading/unloading cycles. The actively cooled areas next to the electrical terminals are clearly visible. Furthermore, a temperature gradient has built up towards the bottom of the cell. The maximum temperature measured during this experiment is 30.1 °C, which is 1.5 °C less than in the first experiment. In other words, when choosing a more appropriate location for the active cooling of the battery cell, the resulting surface temperature gradient can be reduced by about 23%.

Table 3. Temperature gradient measured along a line on the surface from top to bottom in the center of the front face ($y = 0$ mm) and the side face ($y = 86.5$ mm) of the battery cell.

Sensor z-coordinate	Front Side@ $y = 0$ mm	Side-Face@ $y = 86.5$ mm
-23.4 mm	31.6 °C	31.5 °C
-48.4 mm	31.6 °C	30.7 °C
-73.4 mm	31.2 °C	30.0 °C
-98.4 mm	30.4 °C	29.0 °C
-123.4 mm	28.9 °C	27.6 °C
-136.0 mm	25.1 °C	25.3 °C

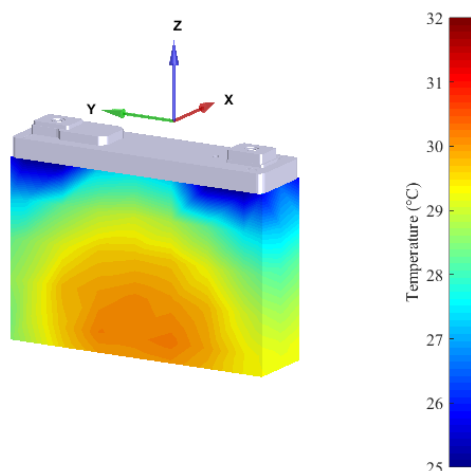


Figure 8. Measured temperature distribution when cooling in direct proximity to the electrical terminals.

This effect becomes even more apparent in the case of the third scenario. Here, the active cooling is placed right in the center of the front and rear face, respectively. Thereby, four THFS units are used on each side. In this case, the maximum temperature gradient can be reduced further to a level as low as 3.6 °C, as shown in Figure 9, which corresponds to a reduction of 40% compared to the first scenario. Obviously, this could be further improved by increasing the actively cooled area on the front and rear faces, which would make sense also from a design point of view. This means, in a real world application, iso-thermal heat sink plates could be located between each pair of battery cells. For the battery cell under investigation, such a configuration would lead to differences in the surface temperature that are literally not measurable.

4. Conclusions

The methodology presented in this paper can be used to perform a thermal characterization of single battery cells. This enables the amount and location of released heat for a given load profile to be obtained as a result. Thereby, it is possible to draw conclusions about the internal structure of a battery cell. With known low thermal resistivity paths, the optimal location for active cooling can be found. The same test setup can be operated in a different mode to verify the effectiveness

of a proposed cooling scheme and to evaluate the resulting temperature gradient on the battery cell surface. This can be accomplished by changing software settings only and without rearranging the battery cell or any other part of the setup. It has been shown that the location of an active cooling system is a crucial point when designing thermal management systems for batteries. For the example presented in this paper, the maximum surface temperature can be reduced by 40% for a given load profile simply by varying the location of the actively cooled areas. Although the internal temperature of the battery cell is not captured, they are supposed to reduce in correlation with the surface temperature. In addition, some work is in progress to use the data from these types of experiments to automatically identify the parameters of a lumped model similar to work presented by Damay et al. [18].

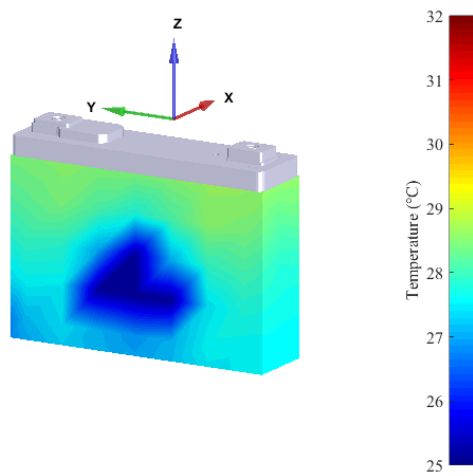


Figure 9. Measured temperature distribution when cooling in the center of the front and rear side, respectively.

At the present time, a mechanically more flexible version of the presented test rig has been built. The distance between the THFS units is adjustable within a range of 25 mm to 75 mm, which allows prismatic and pouch cells of various sizes to be accommodated. In addition, a system is under development to measure and control the heat transferred through the external electrical connectors. This is a necessary measure in order to improve the accuracy of the overall system. During the experiments presented in this paper, it was found that, in some cases, heat is not only released through the electrical connections, but also delivered towards the battery, due to resistive losses and Peltier effects at the electrical connections. Additionally, work is in progress to downsize the THFS units in such a way that they can be applied on 18,650 cylindrical cells. Besides the miniaturization itself, the main challenge is the low power dissipation of small sized cells.

A challenge inherent to the presented test method is the fact that it is not possible to cover the entire surface of a battery cell with active THFS units. This is mainly for practical reasons, such as the need for packaging and cabling. Another restriction for the arrangement presented here is the fact that zero distance between the copper plates of adjacent THFS units would lead to a thermal short cut and hence to an averaging of the temperature distribution. Therefore, the sensing elements of the THFS unit have to be framed. Thereby, some of the internally generated heat bypasses the sensor and is not captured by the test setup. In order to account for this, the heat loss between the THFS units needs to be minimized, which is accomplished by encapsulating the measurement units with insulating foam. Furthermore, the remaining heat loss will be estimated using a finite element model of a test scenario with a dummy battery cell made of a known material. To do this, a temperature gradient across a stainless steel block is obtained by setting the desired temperature of the THFS units on two opposing sides to different values (e.g., 15 °C and 25 °C). The remaining THFS units are operated in mode 2 and control the heat flux to be zero. In the finite element model (FEM), the exact

same boundary conditions and material properties are used. The model is then used to tune the equivalent heat conductivity of the insulating foam in such a way that the calculated temperature gradient matches the measured values. This allows for a compensation of parasitic heat flux and will increase the overall accuracy of the method presented.

Acknowledgments: This work was funded by the Swiss Commission for Innovation and Technology (CTI) under the “SCCER Efficient Technologies and Systems for Mobility” Program. The authors wish to thank the colleagues from the Institute for Electronic, Sensors and Actuators, especially Adrian E. Weitnauer, for their support in designing the multi-channel power stage. A further thanks goes to our colleagues from the SCCER network for valuable discussions on the topic.

Author Contributions: Gerhard Rizzo conceived and designed the experiments. Alfred Gadola conducted the mechanical design, assembled the test rig and performed the experiments. Rouven Christen wrote the software and control algorithms needed to operate the test rig. Gerhard Rizzo and Rouven Christen analyzed the data and wrote the paper. Max Stöck contributed to the paper structure and overall idea.

Conflicts of Interest: The authors declare no conflict of interest.

References

1. Sasaki, T.; Ukyo, Y.; Novák, P. Memory effect in a lithium-ion battery. *Nat. Mater.* **2013**, *12*, 569–575.
2. Waldmann, T.; Wilka, M.; Kasper, M.; Fleischhammer, M.; Wohlfahrt-Mehrens, M. Temperature dependent ageing mechanisms in lithium-ion batteries—A Post-Mortem study. *J. Power Sources* **2014**, *262*, 129–135.
3. Bloom, I.; Jones, S.A.; Polzin, E.G.; Battaglia, V.S.; Henriksen, G.L.; Motloch, C.G.; Wright, R.B.; Jungst, R.G.; Case, H.L.; Doughty, D.H. Mechanisms of impedance rise in high-power, lithium-ion cells. *J. Power Sources* **2002**, *111*, 152–159.
4. Vetter, J.; Novák, P.; Wagner, M.R.; Veit, C.; Möller, K.C.; Besenhard, J.O.; Winter, M.; Wohlfahrt-Mehrens, M.; Vogler, C.; Hammouche, A. Ageing mechanisms in lithium-ion batteries. *J. Power Sources* **2005**, *147*, 269–281.
5. Troxler, Y.; Wu, B.; Marinescu, M.; Yufit, V.; Patel, Y.; Marquis, A.J.; Brandon, N.P.; Offer, G.J. The effect of thermal gradients on the performance of lithium-ion batteries. *J. Power Sources* **2014**, *247*, 1018–1025.
6. Gogoana, R.; Pinson, M.B.; Bazant, M.Z.; Sarma, S.E. Internal resistance matching for parallel-connected lithium-ion cells and impacts on battery pack cycle life. *J. Power Sources* **2014**, *252*, 8–13.
7. Abdul-Quadir, Y.; Laurila, T.; Karppinen, J.; Jalkanen, K.; Vuorilehto, K.; Skogström, L.; Paulasto-Kröckel, M. Heat generation in high power prismatic Li-ion battery cell with LiMnNiCoO₂ cathode material. *Int. J. Energy Res.* **2014**, *38*, 1424–1437.
8. Bernardi, D.; Pawlikowski, E.; Newman, J. A general energy balance for battery systems. *J. Electrochem. Soc.* **1985**, *132*, 5–12.
9. Chen, K.; Unsworth, G.; Li, X. Measurements of heat generation in prismatic Li-ion batteries. *J. Power Sources* **2014**, *261*, 28–37.
10. Veth, C.; Dragicevic, D.; Merten, C. Thermal characterizations of a large-format lithium ion cell focused on high current discharges. *J. Power Sources* **2014**, *267*, 760–769.
11. Lin, C.; Xu, S.; Li, Z.; Li, B.; Chang, G.; Liu, J. Thermal analysis of large-capacity LiFePO₄ power batteries for electric vehicles. *J. Power Sources* **2015**, *294*, 633–642.
12. Murashko, K.A.; Mityakov, A.V.; Pyrhönen, J.; Mityakov, V.Y.; Sapozhnikov, S.S. Thermal parameters determination of battery cells by local heat flux measurements. *J. Power Sources* **2014**, *271*, 48–54.
13. Mckinnon, C.; Bernardini, R.R.; Thresher, W.; Ruis, S.L.; Yarbrough, D.W. Commercial bismuth telluride-based Peltier plates for use as heat flux transducers. *AIRAH Ecolibrium* **2010**, *32*–36.
14. Rowe, D.M. *CRC Handbook of Thermoelectrics*; CRC Press: Boca Raton, FL, USA, 1995.
15. Lineykin, S.; Ben-Yaakov, S. Modeling and analysis of thermoelectric modules. *IEEE Trans. Ind. Appl.* **2007**, *43*, 505–512.
16. Liu, G.; Ouyang, M.; Lu, L.; Li, J.; Han, X. Analysis of the heat generation of lithium-ion battery during charging and discharging considering different influencing factors. *J. Therm. Anal. Calorim.* **2014**, *116*, 1001–1010.

17. Pavoni, F. The Lithium-Battery Value Chain. Available online: http://www.icatconf.com/Sunumlar/SESSION4/3_LiB-Market-Overview-SHORT_2012-08-03_TR%20version.pdf (accessed on 4 January 2017).
18. Damay, N.; Forgez, C.; Bichat, M.P.; Friedrich, G. Thermal modeling of large prismatic LiFePO₄/graphite battery. Coupled thermal and heat generation models for characterization and simulation. *J. Power Sources* **2015**, *283*, 37–45.



© 2017 by the authors; licensee MDPI, Basel, Switzerland. This article is an open access article distributed under the terms and conditions of the Creative Commons Attribution (CC BY) license (<http://creativecommons.org/licenses/by/4.0/>).